

DESY SR-81/03
June 1981

Eigentum der Property of	DESY	Bibliothek library
Zugang: Accessions:	26. AUG. 1981	
Leihfrist: Loan period:	7	Tage days

LAUE PHOTOGRAPHY OF FINE CRYSTALLINE PARTICLES

by

U. Asaf, Z. H. Kalman, I. T. Steinberger

Racah Institute of Physics, The Hebrew University, Jerusalem, Israel

W. Graeff

*Hamburger Synchrotronstrahlungslabor HASYLAB
at
Deutsches Elektronen-Synchrotron DESY, Hamburg*

DESY behält sich alle Rechte für den Fall der Schutzrechtserteilung und für die wirtschaftliche Verwertung der in diesem Bericht enthaltenen Informationen vor.

DESY reserves all rights for commercial use of information included in this report, especially in case of apply for or grant of patents.

To be sure that your preprints are promptly included in the
HIGH ENERGY PHYSICS INDEX,
send them to the following address (if possible by air mail) :

DESY
Bibliothek
Notkestrasse 85
2 Hamburg 52
Germany

Laue photography of fine crystalline particles

I.T. Steinberger*, U. Asaf*, W. Graeff** and Z.H. Kalman*.

* Racah Institute of Physics, The Hebrew University, Jerusalem, Israel.

** Deutsches Elektronen Synchrotron, Hamburg, F.R.G.

Abstract

An experimental method is described for the determination of crystallite dimensions in polycrystalline materials. It is based on studying the geometry of streaks that appear in powder photographs taken with white x-ray radiation. A detailed analysis is presented that includes a differentiation between these streaks and somewhat similar streaks due to asterism. Results by synchrotron radiation from powder samples of various materials are discussed and compared with the crystallite dimensions obtained by other methods. It is demonstrated that the method is largely complementary to measurements by electron microscopy and that it is particularly useful for the determination of the thickness distribution of thin (0.005-0.5 μm) platelets, oriented parallel to the substrate.

to be published in J. Appl. Cryst:

I. Introduction

Serious efforts were made in the early 1950's to obtain the size distribution of crystalline powders by using x-ray microbeam techniques (Hirsch & Kellar, 1951; Hirsch 1956). In practice the methods led to the determination of the average dimensions only. The very long exposure times needed with the sources then available as well as the progress of electron microscope techniques discouraged further development.

With the availability of the intense and well-collimated synchrotron radiation sources utilization of white x-ray radiation for crystallite size determination became feasible. It has been recently shown (Kalman, Steinberger and Hasnain, 1979) that the Laue spots deviate from the geometric projections of the crystallites for small crystals ("size effect"). In fact, if the dimension roughly parallel to the direction of incident radiation is small, the Laue spots become radial streaks pointing to the centre; the lengths and widths of the streaks are inversely proportional to certain crystallite dimensions. The development of these streaks during crystal growth and recrystallization was illustrated for the case of xenon and krypton crystals.

Roughly radial streaks in a Laue photograph can appear because of another reason, namely strain gradients that involve bending of the crystal ("asterism", Barrett 1952). In this paper a systematic theoretical comparison will be given between the features of the size effect and those of asterism.

Laue reflection photographs from polycrystalline powders (mostly oxides) were taken at the DESY laboratory for synchrotron radiation in Hamburg. The synchrotron radiation work was complemented in Jerusalem by a direct study of the crystal morphology, using scanning electron microscopy (SEM) and transmission electron microscopy (TEM). Occasionally "conventional" Laue photographs

were also taken from the powders with a fine-focus x-ray source. The studies led to an assessment of the feasibility of Laue photography of powders ("LPP") for crystallite dimension determination.

II. Theory

In order to compare the shape of a reflection spot obtained from a small but perfect crystallite to that obtained from a bent but not necessarily small one we will consider reflections from lattice planes having unit normals \underline{n} , with polychromatic radiation impinging on the plane at the angle α . α is the Bragg angle for a wavelength λ contained in the primary spectrum. $\underline{S}_0 = \underline{j}$ is the unit vector in the direction of the incident radiation and \underline{S} the unit vector in the direction of the specular reflection:

$$\underline{S} = \underline{S}_0 - 2(\underline{S}_0 \cdot \underline{n})\underline{n} \quad \dots\dots 1a$$

The axis \underline{j} is chosen in such a way (see Fig. 1) that

$$\underline{n} = \cos\alpha \underline{j} - \sin\alpha \underline{i} \quad \dots\dots 1b$$

We shall consider separately the two cases: that of asterism and that of a small crystallite.

A. Asterism

Consider the reflection from a crystallite sufficiently large, so that diffraction broadening due to its size may be neglected. The crystallite is assumed to be cylindrically bent, so that the normal to the reflecting plane varies between two limiting directions, say \underline{n} and \underline{n}' . The orientation of \underline{n}' is expressed by the polar angles ψ and ϕ (Fig. 2).

We have then, for the components ξ' η' ζ' of \underline{n}' in the coordinate system \underline{i} \underline{j} \underline{k}

$$\xi' = -\cos\psi \sin\alpha + \sin\psi \cos\phi \cos\alpha \quad \dots\dots 2a$$

$$\eta' = \cos\psi \cos\alpha + \sin\psi \cos\phi \sin\alpha \quad \dots\dots 2b$$

$$\zeta' = \sin\psi \sin\phi \quad \dots\dots 2c$$

For the original direction of the normal $\phi = \psi = 0$ and we have

$$\xi = -\sin\alpha \quad \dots\dots 3a$$

$$\eta = \cos\alpha \quad \dots\dots 3b$$

$$\zeta = 0 \quad \dots\dots 3c$$

The direction of the reflected ray of the bent crystal will be given by the unit vector

$$\underline{S}' = \underline{S}_0 - 2(\underline{S}_0 \cdot \underline{n}')\underline{n}' \quad \dots\dots 4$$

The photographic film is placed at a distance D from the crystal perpendicularly to the incident beam (Fig. 1). The reflection on the film will appear as a streak between the limiting positions \underline{R} and \underline{R}' (referred to the site of the crystal), corresponding to the normals \underline{n} and \underline{n}' respectively:

$$\underline{R} = \frac{D}{(\underline{S} \cdot \underline{i})} \cdot \underline{S} \equiv x\underline{i} + y\underline{j} + z\underline{k} = D \left(\underline{i} - \frac{2\xi\eta}{1-2\xi^2} \underline{j} \right) \quad \dots\dots 5a$$

$$\underline{R}' = \frac{D}{(\underline{S}' \cdot \underline{i})} \cdot \underline{S}' \equiv x'\underline{i} + y'\underline{j} + z'\underline{k} = D \left(\underline{i} - \frac{2\xi'\eta'}{1-2\xi'^2} \underline{j} - \frac{2\xi'\zeta'}{1-2\xi'^2} \underline{k} \right) \quad \dots\dots 5b$$

Accordingly, substitution from 2 and 3 into 5a and 5b yields the following rather unwieldy expressions for $y'-y$ and $z'-z$, the radial and tangential components respectively of the reflection streak:

$$\frac{y'-y}{D} = \tan 2\alpha - \frac{2(\cos\psi\cos\alpha + \sin\psi\cos\phi\sin\alpha)(-\cos\psi\sin\alpha + \sin\psi\cos\phi\cos\alpha)}{1-2(-\cos\psi\sin\alpha + \sin\psi\cos\phi\cos\alpha)^2} \dots\dots\dots 6a$$

$$\frac{z'-z}{D} = \frac{-2 \sin\psi\sin\phi(-\cos\psi\sin\alpha + \sin\psi\cos\phi\cos\alpha)}{1-2(-\cos\psi\sin\alpha + \sin\psi\cos\phi\cos\alpha)^2} \dots\dots\dots 6b$$

If δ is the angle of deviation from the radial direction then $\delta = \frac{z'-z}{y'-y}$ 6c

The normalized length of the streak $\lambda = |R'-R|/D$ is given by $\lambda = \sqrt{(y'-y)^2 + (z'-z)^2}/D$ 6d

λ and δ , as calculated from equations 6a-6d are presented in Fig. 3 as a function of the azimuth angle ϕ for a fixed glancing angle α and three different bending angles ψ . Analysis of the figure and of equations 6a-6d yields the following qualitative conclusions:

a) For constant α and ϕ $y'-y$ increases proportionally with $z'-z$, provided the bending angle ψ is small. In other words for small ψ the streaks are straight. For larger ψ the streaks become somewhat curved. To quote a rather extreme case of arching, we note that for $\phi = 80^\circ$ and $\alpha = 15^\circ$ the direction of the streak varies by about 10° if ψ varies from 0° to 6° . For smaller values of α and ϕ the streaks are less curved.

b) The streak length λ decreases monotonously with the increase of ϕ and with the decrease of α . For small ψ , λ is proportional to ψ . Note that the range of variation of λ with ϕ is due to the variation of the direction of the bending axis in the plane perpendicular to the beam. In a sample consisting of many platelets

all perpendicular to the incident beam and dispersed on a substrate, the various directions of bending should be equally probable and therefore the whole range of variation of λ with ϕ should be readily observable. For small glancing angles α , λ decreases by about a factor of ten if ϕ varies from 0° to 90° . The range is smaller for larger α , e.g., for $\alpha = 15^\circ$ λ varies by less than a factor of 5. These ranges are insensitive to the actual value of ψ .

c) The deviation δ of the streak from the radial direction (neglecting the arching) increases with increasing ϕ , the more so the greater the value of α . For given α and ϕ , δ increases slightly with the decrease of ψ . As the deviation from radiality is an important characteristic property of asterism, Table 1 presents the expected frequency of occurrence of δ within given limits, assuming that all values of ϕ appear with equal probability. It should be particularly noted that even under conditions most favorable for radial streaks ($\psi=5^\circ$, $\alpha=5^\circ$), at least 20% of the streaks should be markedly off-radial, i.e., $\delta > 10^\circ$. In the other cases presented the percentage of markedly off-radial streaks is considerably larger, reaching even more than 50%. Most of these off-radial streaks are of lengths comparable with those of the radial ones (see also fig. 3).

With the assumption $\psi \ll 1$ a useful first approximation can be obtained for $\tan\delta$:

$$\tan\delta = -\sin(\alpha-\psi)\cos\alpha\tan\phi \dots\dots\dots 6e$$

If one assumes further that $\psi \ll \alpha$ one has the following approximate relations:

$$\frac{y'-y}{D} = -\frac{2\psi\cos\phi}{\cos^2 2\alpha} = -\psi\cos\phi \frac{d(\tan 2\alpha)}{d\alpha} \quad \dots\dots 7a$$

$$\frac{z'-z}{D} = \frac{2\psi\sin\phi\sin\alpha}{\cos 2\alpha} \quad \dots\dots 7b$$

$$\tan\delta = -\sin\alpha\cos 2\alpha\tan\phi \quad \dots\dots 7c$$

The geometrical meaning of Eq. 7a is immediately clear if one takes into account that $-\psi\cos\phi$ is the projection of the angle between the normals \underline{n} and \underline{n}' on the original plane of incidence xy (Fig. 2). All the features of asterism noted above can be easily seen by analysing equations 7a-7b. One should note that if bending takes place about one axis only, as considered above, there will be no broadening of the diffraction streak.

B. Size effect

Following the detailed paper on this subject (Kalman, Steinberger & Hasnain, 1979) we consider an (H 0 0) reflection from a perfect orthorhombic crystal. For simplicity, the crystal is considered to be shaped as a rectangular parallelepiped of edge lengths A_1, A_2, A_3 . The edges are parallel to the elementary lattice translations $\underline{a}_1, \underline{a}_2, \underline{a}_3$. Let the incident beam direction be parallel to \underline{a}_1 and assume that A_2, A_3 are small. The relaxation of the Bragg condition causes then the appearance of a broadened, exactly radial streak. Denote by α the glancing angle and λ_α the corresponding wavelength that satisfies the Bragg condition exactly. The reflected beam has then an angular extension $\pm\Delta\eta$ in the plane of incidence and $\pm\Delta\epsilon$ in the plane perpendicular to it, resulting in a

streak of length $y'-y$ and breadth $z'-z$ on the film. If $\Delta\eta$ is small enough to write $\sin\Delta\eta \approx \Delta\eta$, one finds from eq. 8b and 8c of Kalman et al., 1979

$$\frac{y'-y}{D} = \Delta\eta \frac{d}{d\alpha} (\tan 2\alpha) = \frac{2\lambda_\alpha}{A_2\sin\alpha\cos^2 2\alpha} = \frac{4d}{A_2\cos^2 2\alpha} \quad \dots\dots 8a$$

$$\frac{z'-z}{D} = \frac{2\Delta\epsilon}{\cos 2\alpha} = \frac{2\lambda_\alpha}{A_3\cos 2\alpha} = \frac{4d\sin\alpha}{A_3\cos 2\alpha} \quad \dots\dots 8b$$

Note that the length of the size effect streak increases slowly with increasing α , due to the geometry of the projection. The same projection geometry holds for the similar relation for asterism, Eq. 7a. The breadth of the size effect streak increases markedly with increasing α .

With polycrystalline and powder samples asterism streaks can be distinguished from the size effect streaks by means of the broadening and the off-radiality. Table 2 presents the main characteristics of the two effects.

C. Combinations of effects.

Diffraction effects similar to those obtained from bent crystallites may result from aggregates of nearly, but not quite, parallel aligned crystallites. Such aggregates may arise either during growth or by breaking up of originally single crystals (e.g. by polygonization). If the component crystallites are large and not strained, the diffraction photograph will show discrete spots. If the misorientation is about a common axis, the spots will be arranged along such streaks as would result from bending about the same axis. If, however, the component crystallites are small or curved or both, the discrete spots will each broaden and merge with neighbouring spots into a single streak, often with a resolvable inner structure.

For asterism it was assumed in the calculation that the angular broadening of a reflection (i.e., the quantity $|S'_m - S_m|$) from a relatively large curved crystallite is determined by geometric factors alone: it is essentially twice the angle ψ subtended by the curved crystallite, modified by the projection geometry (Eg. 7a). The question arises whether additional broadening should be expected due to the fact that the lattice curvature may decrease the size of the coherently reflecting regions within the crystallite and hence cause an additional size broadening. Quantitative analysis of this situation (Kalman, 1981) shows however that the angular width of the reflection is indeed very closely equal to 2ψ : there is some additional broadening $\delta\psi$ of the order of $\delta\psi \sim (\lambda\rho/\sin\alpha)^{1/2}$, where ρ is the curvature. Clearly, $\delta\psi$ is negligible compared with ψ for any reasonable value of ρ .

Size effect and asterism may appear concurrently in thin bent crystals, e.g., in the case of reflections from planes approximately perpendicular to the main plane of a bent platelet. A linear superposition of the two effects occurs: The length of the streaks is approximately equal to the sum of lengths predicted by the two effects. The deviation from radiality is less than expected from asterism alone, since both effects contribute to the radial component (y-direction), but only asterism contributes to the tangential one (z-direction).

For "pure" asterism, only one bending axis was considered for each crystallite, assuming that in more complicated cases the bending that corresponds to the largest curvature will be dominant. Strongly curved streaks may appear for a heavily strained multiply bent crystallite. Since the emphasis in this work is on the size effect, these more involved cases of asterism will not be considered.

III. Experimental

Commercially available powder samples of elements or simple compounds were used in most experiments. It was assumed that during manufacture the samples did not undergo any drastic mechanical treatment, like milling, grinding, etc., and thus the crystallites were not severely strained. The slight or even totally absent asterism found in the experiments (see below) justified this assumption. In many cases the powder was spread dry on a thin mylar substrate and held there by electrostatic attraction only. Compact samples, with the powder densely covering the substrate, were obtained in this manner. To prepare a dispersed sample, a small amount of powder was mixed into a test tube containing water or another dispersive agent. After some agitation, a droplet of the mixture was deposited on the mylar substrate and let dry. In all cases each powder particle was, in fact, an aggregate of crystallites; this was seen by SEM and TEM. These aggregates were broken up into smaller ones by the dispersion procedure. Moreover, in the dispersed samples the individual particles became separated from each other and thus the substrate was covered only sparsely.

Laue photographs of the powder samples ("LPP") were taken using polychromatic synchrotron radiation at the DORIS storage ring of DESY, Hamburg. The beam passed a pinhole made of the usual lead-iron-aluminium combination. For the photographs the sample was placed in a vacuum chamber carefully shielded from stray radiation. A flat x-ray film, placed behind the sample, served to record the reflections. When dispersed powder samples were used, a chosen particle (or particles) was brought in the beam path by means of a simple manipulator and a microscope.

The SEM studies were made with the JEOL-35 instrument of the School of Applied Sciences of the H.U. The samples for these studies were usually prepared by spraying the powder on an aluminium substrate coated by an adhesive. Dispersed samples for SEM were prepared simultaneously with the corresponding dispersed samples intended for LPP, on the same (mylar) substrate and in an identical fashion. In all cases the samples for SEM were coated by a sputtered layer of gold. The TEM measurements were performed using the JEOL-200CX instrument of the Institute of Life Sciences of the H.U. The samples for TEM were always dispersed by suspending the powder in water and gently agitating the mixture in a supersonic bath. The samples for TEM were obtained finally on a formvar substrate; they were not coated.

IV. Results

The various powder samples had been chosen for study in the expectation that the samples would differ among them in crystallite dimensions, shapes and orientations and thus the experiments would lead to a practical assessment of the LPP in various cases. Special attention was paid to possible contributions of asterism. The following presentation starts with the case that turned out to be the simplest one and progressing gradually to more involved ones. In each case the description of the LPP results is followed by the conclusions from the control experiments by TEM, electron diffraction and SEM. Scores of photographs of each kind were taken; the following is a representative sample.

BaSO₄

This powder was specially prepared for the present experiments by the courtesy of Prof. S. Sarig of the Casali Institute of Applied Chemistry of the H.U., with the intent to obtain a reasonably uniform size distribution. She employed controlled precipitation from solution of $2 \times 10^{-2} \text{M}$ BaCl₂ and $2 \times 10^{-2} \text{M}$ Na₂SO₄.

Fig. 4 presents a part of a Laue powder photograph obtained at DESY. Numerous streaks are seen, almost all exactly radial, with very few exceptions. Even the off-radial streaks are deviating only very slightly from the radial direction. It follows that the streaks must be due to size effect and not to asterism; the very rarely observed slight off-radiality is due to a superposition of slight asterism on the size effect. The streaks look roughly uniform in length; there is no obvious effect of the distance r from the centre (in other words, no effect of the glancing angle α) on the lengths. On the other hand, the streaks become broader with increasing r . These facts are in full accord with the predictions of eq.8 for the dependencies of the streak lengths and breadths on α , provided all streaks are due to reflections corresponding to similar d -values.

For quantitative deductions from the LPP, the distance from the centre r on the film was calibrated in terms of λ by means of the Bragg relation. For this purpose, a zirconium filter was put on one half (not shown) of the photographic film and note was made of the positions of the dark rings ("eclipsed Debye-Scherrer rings", Kalman et al, 1979) formed at the positions of the reflections with the principal d -values of BaSO₄ and the K-edge of Zr(0.6877Å). This furnished the proportionality factor between $\tan 2\alpha$ and r .

From the measurement of the lengths of a few dozen streaks and using eq.8a, the effective thickness distribution of the crystallites was established.

A_2 in Eq.8a correspond now to the effective thickness t , i.e., the path length of the incident radiation within the crystallite. It was found that the distribution has one peak around $0.05 \mu\text{m}$, with a half width of about $0.02 \mu\text{m}$.

The quantitative evaluation of the lateral dimensions a of the crystallite (corresponding to A_3 in eq.8b) from the streak breadths is somewhat more involved, because of the presence of many broad streaks that are stronger than the majority. The combination of broadness and high intensity eliminates the possibility of size effect broadening, since thin crystals of small lateral dimensions can yield only weak reflections because of the small volume involved. It seems that the broadening of the strong streaks is due to overexposure, though some resolved superpositions of reflections from almost exactly parallel crystallite aggregates (see the case of MnO_2 below) cannot be ruled out either. The breadths of the rest of the streaks indicate lateral dimensions varying from 0.08 to $0.4 \mu\text{m}$.

Fig. 5 shows a TEM photograph of a typical BaSO_4 crystallite. It is seen that it is a dendritic flake; the partial transparency to electrons shows that it is rather thin. All crystallites were such flakes and all were oriented with their main plane parallel to the substrate.

The flake thickness was directly determined by observing projections of holes in the flakes with the sample tilted (45° in Fig. 6). Such measurements yielded thicknesses of 0.15 - $0.1 \mu\text{m}$, in reasonable accord with the conclusions from the

LPP. The TEM results also show that the approximate uniformity of the LPP streak lengths is due to the approximately uniform thickness of the flakes and their consistent orientation parallel to the substrate.

The lateral dimensions of a single crystal could not be determined conclusively. On one hand Fig. 5 seems to indicate that each flake consists of numerous small crystals, with $0.2 \mu\text{m} < a < 1 \mu\text{m}$. However, electron diffraction of individual flakes (Fig.7) shows that each flake consists of only a few, say a dozen, single crystals. This would put the probable limits higher, namely $0.5 \mu\text{m} < a < 5 \mu\text{m}$. Comparison of the two estimates with the LPP results indicate that the crystallites included in the flakes can vary considerably in their lateral dimensions, probably because of imperfect crystallization. It should be emphasized again that the upper limit for the lateral dimensions a , as obtained from LPP, is certainly incorrect, and it should be higher: larger crystals cause overexposure and the breadth measurement becomes impossible.

MnO_2 (Baker).

The LPP of this powder (Fig.8, compact sample) shows many streaks, almost all exactly radial. It follows that this is also a clear case of size effect. The lengths of the streaks vary widely. The wavelength calibration was obtained by means of the K-edges of the silver and the bromine in the photographic emulsion. Evaluation of the effective thicknesses from the streak lengths yields $0.015 \mu\text{m} < t < 0.25 \mu\text{m}$ with a rather flat peak of the distribution curve at about $0.03 \mu\text{m}$. The streak breadths also vary widely, ranging from the instrumental width ($0.03 \mu\text{m}$) to very thick ($\sim 1 \mu\text{m}$). Careful inspection shows that most of the very thick streaks are composed of a few parallel or almost parallel streaks; several examples

for this phenomenon are seen in fig. 8. Even so, many of the very thick streaks are strongly overexposed. From measurements of the breadth of the other streaks it is found that $a > 0.2 \mu\text{m}$. The upper limit for a cannot be stated since the corresponding streak breadth would be less than the instrumental breadth of the streaks, but this limit is certainly above $1 \mu\text{m}$.

SEM of compact samples (Fig.9) does not yield clear conclusions: at first sight it seems that the sample is composed of thick blocks, with a comparable t , but closer inspection indicates substructure within the blocks. TEM of a dispersed sample reveals that the substructure is, indeed, real: it shows platelets usually piled in small stacks, one atop the other, approximately parallel to the substrate. Some stacks and individual platelets are, however, inclined to the surface. These platelets present a longer effective path for the x-radiation in the LPP experiment. This explains the wide variation of t and a as obtained from the LPP.

The lateral dimensions of the platelets was determined by TEM, they were found to be between the limits $0.2 \mu\text{m} < a < 10 \mu\text{m}$. Comparing this with the LPP result above shows that the larger crystallites did not yield, indeed, narrow streaks, but caused overexposure and therefore broadening. In one case it was possible to observe a platelet approximately "edge on" by TEM. Its thickness was found to be about $0.03 \mu\text{m}$. Individual platelets gave single-crystal electron diffraction patterns.

The formation of small stacks of platelets, as shown by TEM, explains the frequent appearance of structure (fine streaks very close together) within the LPP streaks (Fig.8): the individual platelets within a stack are not fully aligned with each other and therefore give slightly different streaks.

Though this is a somewhat more involved case than that of BaSO_4 , the conclusions from LPP are fully vindicated by SEM and TEM. It should be noted that the range of the effective thickness could be established by LPP only.

Pb_3O_4 (M&B)

Two LPP's are presented, obtained from samples prepared in different ways from the same powder. Fig. 10 refers to a compact sample, the beam traversing a very large number of crystallites, while for Fig.11 the sample was dispersed and only a few grains (each containing several crystallites, as it eventually turned out) were in the beam path. Comparison of the two figures shows the following differences: a) On fig. 10 the density of spots is so high that it is very difficult to observe the shapes and dimensions of individual spots. Individual spots and streaks can be conveniently studied by means of fig. 11. b) In fig. 11 there is no indication for eclipsed Debye-Scherrer rings, useful for wavelength calibration. Such rings are clearly seen in fig. 10. They are due to the K-edges of silver and bromine contained in the photographic emulsion. c) In fig. 10 there is a continuous background halo as well, caused by many crystallites that are too small to yield distinct reflections. There is no indication for a halo in Fig. 11, as there were not enough small crystallites in the beam.

The majority of the streaks (Fig. 11) are radial, but there is a non-negligible number of off-radial streaks as well. Still, the dominant effect must be the size effect since strongly off-radial streaks are very rare and short. Thus the off-radiality of some streaks is most likely to be due to slight bending of thin crystals. Analysis of the streak lengths yields for the effective thickness

$0.02 \mu\text{m} < t < 0.5 \mu\text{m}$. The distribution of thicknesses is roughly uniform within most of this very wide range. From the breadths of streaks one finds $0.03 \mu\text{m} < t$; the upper limit cannot be determined, as explained for the previous cases, but it is at least $1.2 \mu\text{m}$. The breadth distribution is also roughly uniform. These flat and wide distributions and the similarities of their limiting values lead to the tentative assumption that the crystallites are platelets of roughly uniform dimensions but oriented in an approximately random manner.

Fig. 12 is a TEM photograph of a typical group of crystallites. It is seen that the crystals are, indeed, platelets, some of them piled one atop the other as in the case of MnO_2 presented above. However, for Pb_3O_4 the crystallites are very often not parallel to the substrate; in fact, all orientations are frequent. The thickness of the platelets was determined on some samples viewed "edge on" and it was found to be about $0.02 \mu\text{m}$. The typical lateral dimension was about $1 \mu\text{m}$. Thus the tentative inference from the LPP photographs that we had platelets of the above dimensions but at random orientation has been confirmed.

As in the case of MnO_2 , the stacked arrangement of some of the platelets (Fig. 12) is observable in the LPP-s as well by the appearance of numerous "double" streaks, of similar lengths, very close and approximately parallel to each other. This feature is much clearer on the original photographs than on their reproductions in Fig. 10 and 11. There is no indication by TEM for the slight angular variation (of the order of one degree of arc) of the reflecting plane normals as indicated by the off-radiality of the streaks. In fact it would be difficult to observe the angular variations by any other means except by LPP. Note that this variation could be caused either by bending or by coalescence of reflections from several platelets stacked together; the effect of stacking with some misorientation can, indeed, be seen from the structure of some streaks that was mentioned above.

Compact samples of four more materials, namely Bi(BDH), MoO_3 (Baker), SiC (Linde, 800) and Te(Johnson and Matthey) yielded LPP-s similar to those of Pb_3O_4 . Again, SEM and TEM photographs indicated that the crystallites consisted of platelets having all possible orientations with respect to the surface. In all cases good agreement was found between the various methods in the determination of the crystallite dimensions, getting more information from LPP about the effective thickness and from SEM and TEM about the lateral dimensions. Only LPP gave direct indications of angular variations of crystal plane normals.

Cu(Baker)

Fig. 13 is an LPP of a compact sample of this material. A strong background halo indicates that the sample includes many crystallites too small to yield distinct streaks. There are also many considerably broadened streaks; these are as a rule, rather faint. It follows that the lateral dimensions a of the crystallites contributing these streaks were also small. There are no broad, overexposed and long streaks in this photograph, thus one can rule out the presence of large platelets roughly perpendicular to the incident beam. All this indicates that the crystallites are roughly spheroidal. Measuring of the lengths and breadths of streaks yielded $0.1 \mu\text{m} < a = t < 0.6 \mu\text{m}$. SEM photographs (Fig. 14) vindicate these conclusions: the crystallites were found to be globular, of diameters ranging from $0.04 \mu\text{m}$ to about $0.3 \mu\text{m}$. Obviously the smallest globules contributed only to the background halo.

LPP of compact samples of Fe_2O_3 powder (polishing agent by Edmond) yielded few, very faint streaks on a continuous background, indicating small crystal dimensions.

If the sample was carefully dispersed, the photographic plate did not darken at all. SEM and TEM photographs showed particles having typical lateral dimensions of 0.2 μm ; their thicknesses could not be estimated reliably.

CeO₂(Amer.Potash)

Fig. 15 shows the LPP of a "compact" sample, containing a very large number of powder particles. Dark haloes are only seen, modulated by intensity variations caused by eclipsed Debye-Scherrer rings associated with the principal d-values of CeO₂ and the K-absorption edge of silver and bromine, contained in the photographic emulsion. One infers from here that we had only very small particles and thus all the streaks washed out and merged together. An attempt was made to observe distinct reflections from the same powder by dispersing it with water. Of this sample, an area containing about a hundred grains was selected and aligned to within the cross section of the beam. However, the radiation diffracted from the grains did not cause any observable darkening.

The SEM photographs of compact samples gave a puzzling result: the sample seemed to consist of rhombohedral crystals, having lateral sizes of 5-10 μm and thicknesses of about 1-2 μm . This result, strongly in variance with the LPP conclusions, is explained by the TEM photographs; they show extremely fine crystals of the approximate dimensions 0.03 μm x 0.03 μm x 0.03 μm ; the rhombohedral blocks are composed of these crystals.

The LPP of compact ZnS(B.A.) and SnO₂(Baker) samples also showed only haloes with eclipsed Debye-Scherrer rings and again no darkening was observed with fully dispersed samples. LPP of compact ZnO(B.D.H.) samples revealed haloes with a few superimposed faint streaks. With dispersed streaks there was no observable darkening in this case either.

V. Discussion

The applicability of the Laue method to obtain the distribution of the dimensions of small crystallites has been discussed above by presenting concrete examples. The main general conclusions are as follows:

- 1) Given a powder sample that yields streaky Laue spots, it is usually possible to state by cursory inspection whether the dominant reason for the occurrence of streak is the size effect or asterism. If there is any asterism, there must be some off-radial streaks; asterism is the dominant factor if there are many marked off-radial streaks having lengths comparable to those of the radial or almost radial ones.
- 2) The preparation of the sample for the experiments is of much relevance, especially the dispersion. To make correct deductions and exploit the method in full, usually more than one sample is needed.
- 3) For some samples consisting of very small crystallites the method fails; compact samples yield only a continuous halo, while dispersed samples do not cause any darkening. Ignoring the relatively small variations in the electron densities of one material to the other, the "critical volume" for photographically observable streaks is about $10^{-4} \mu\text{m}^3$; for a somewhat smaller volume, ($6 \times 10^{-5} \mu\text{m}^3$, Cu), no streaks appeared and for larger volumes (starting from $3 \times 10^{-4} \mu\text{m}^3$ in BaSO₄) the streaks were always clearly seen. For standard laboratory x-ray sources this critical volume is larger by at least a factor of ten, as we inferred from preliminary experiments.

The case of Fe_2O_3 is anomalous; the reason might be extremely poor crystallinity

4) Careful scrutiny of the photographs can reveal further features of the texture of the powders, even before starting the measurements of the lengths and the breadths of the streaks. E.g. one gets immediately an impression about the uniformity of the streaks and thus about the uniformity of the effective crystallite dimensions. Moreover, certain arrangements of crystallites, like the formation of small stacks of platelets, are apparent from the photographs.

5) Quantitatively, the measurement of lengths is more reliable than the measurement of breadths (e.g. overexposure problems are much less severe). Thus it is the effective thickness distribution that can be most readily measured. This is a rather significant quantity especially in cases of samples composed of thin (0.005 μm to 0.1 μm) platelets all parallel to the substrate. It would be rather difficult to establish this distribution by other methods: e.g., the use of transmission electron microscopy would involve painstaking measurements on many crystallites.

6) In several ways this method complements known measuring techniques of small particles. All kinds of microscopy establish essentially particle sizes, and auxiliary measurements (usually electron diffraction) are needed to check, whether the individual particles are single crystals or not, while the LPP refers directly to the crystallites. Microscopic techniques deal with individual particles; LPP deals with the statistical distribution of the thickness (or lateral dimensions) of many crystallites. Electron microscopy is most useful in yielding lateral dimensions, while the most significant information obtainable from LPP is the thickness of the samples. The use of x-rays in LPP is particularly advantageous when the samples have to be kept at inconvenient pressures and/or temperatures

and if they have to be enclosed in a cell (Kalman, Steinberger, Hasnain, 1979). Slight bending of crystallites is clearly discerned by LPP but not by TEM.

Acknowledgements

The authors wish to express their thanks to Prof. S. Sarig for preparing the BaSO₄ samples. They thank the staffs of the SEM and TEM units of the H.U. for their help, and A. Drachsler, FRPS, for high quality photographic work.

The authors thank the Director of DESY for the use of the synchrotron radiation facilities and colleagues at this facility for their interest and help. I.T.S. acknowledges the partial support of the MINERVA foundation.

* * * * *

References

BARRETT, C.S.(1952). Structure of Metals, 2nded., pp.414-420, 553-557. New York Toronto, London: McGraw-Hill.

HIRSCH, P.B.(1956) Mosaic Structures in Progress in Metal Physics, edited by Br. Chalmers & R. King, pp.236-339. London&New York: Pergamon Press;

HIRSCH, P.B. and KELLAR J.H.(1951), Proc. Phys. Soc. B.64, 369-374;

KALMAN, Z.H., J. Appl. Cryst., in preparation.

KALMAN, Z.H., STEINBERGER, I.T. & HASNAIN, S.S.(1979), J. Appl. Cryst.12, 525-53

Table 1. The distribution of the angle of deviation δ for various glancing angles α and bending angles ψ , expressed as percentages.

Range of δ	$0^\circ-10^\circ$	$10^\circ-20^\circ$	$20^\circ-30^\circ$	$30^\circ-40^\circ$	$40^\circ-50^\circ$	$50^\circ-60^\circ$	$60^\circ-70^\circ$	$70^\circ-80^\circ$	$80^\circ-90^\circ$
α									
ψ									
5°									
1°	72.2	13.3	5.2	2.8	1.9	1.4	1.1	1.1	1.0
2°	75.1	11.4	4.7	2.7	1.8	1.3	1.2	1.0	0.8
5°	72.3	8.4	3.9	2.3	1.7	1.3	1.0	1.0	0.6
10°									
1°	54.5	19.7	8.8	5.1	3.4	2.7	2.1	2.0	1.7
2°	56.7	18.5	8.3	5.0	3.3	2.6	2.1	2.0	1.5
5°	62.8	15.2	7.2	4.3	3.1	2.5	2.1	1.9	0.9
15°									
1°	44.0	21.8	11.2	6.8	4.7	3.6	3.0	2.6	2.3
2°	45.8	21.2	10.8	6.5	4.5	3.6	2.9	2.7	2.0
5°	50.9	19.1	9.7	6.0	4.3	3.4	2.8	2.7	1.1

Table 2. The main features of the asterism streaks (uniaxial bending) and of the size effect streaks.

Property	Asterism	Size effect
Shape	Approximately straight lines, the curvature increases with increasing glancing angle α	Straight lines
Radiality	Approximately radial	Exactly radial
Breadth width	Determined by the instrumental resolution -no broadening	Broadening increases with the decrease of the lateral dimensions and with the increase of α

Figure captions

Fig. 1. Geometry of a reflection with the glancing angle α , indicating the radial unit vector \underline{j} and tangential unit vector \underline{k} on the film.

Fig. 2. The relationship of the unit vectors \underline{i} , \underline{j} , \underline{k} (fig. 1) to the angles α , ψ and ϕ in asterism.

Fig. 3. Asterism: streak length l and angle of deviation from radiality δ as a function of the azimuth ϕ for three values of α .

Fig. 4. Laue powder photograph of a $BaSO_4$ sample. Source: DORIS at 3.7 GeV, 10 mA. Exposure time: 2 hours.

Fig. 5. Transmission electron micrograph of a $BaSO_4$ flake, 200 kv.

Fig. 6. As fig. 5, but at higher magnification. The stage is tilted to facilitate estimation of the thickness of the flake from the inner walls of the hole.

Fig. 7. Electron diffraction of the flake of fig. 5, 200 kv.

Fig. 8. Laue diffraction photograph of a compact MnO_2 sample. DORIS at 3.185 GeV, 95mA. $3\frac{1}{2}$ min.

Fig. 9. Scanning electron micrograph of a compact MnO_2 sample, 2.5 kv.

Fig. 10. Laue powder photograph of a compact Pb_3O_4 sample. DORIS at 3.185 GeV, 70mA, 1 min.

Fig. 11. Laue powder photograph of a dispersed Pb_3O_4 sample. DORIS at 3.75 GeV, 12mA. 40 min.

Fig. 12. Transmission electron micrograph of Pb_3O_4 crystallites, showing several plates stacked parallel to each other and some almost perpendicular ones, 200 kv.

Fig. 13. Laue powder photograph of a compact Cu sample. DORIS at 3.185 GeV, 83mA. 0.5 min.

Fig. 14. Scanning electron micrograph of compact Cu particles. 25kv.

Fig. 15. Laue powder photographs of a compact CeO_2 sample. DQRIS at 3.185 GeV, 50mA. 1 min.

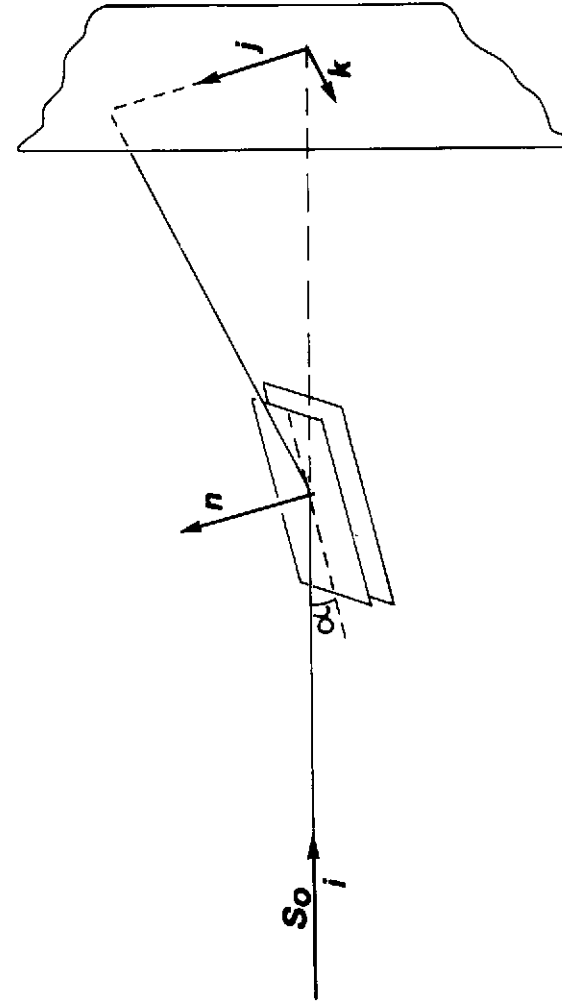


Fig. 1

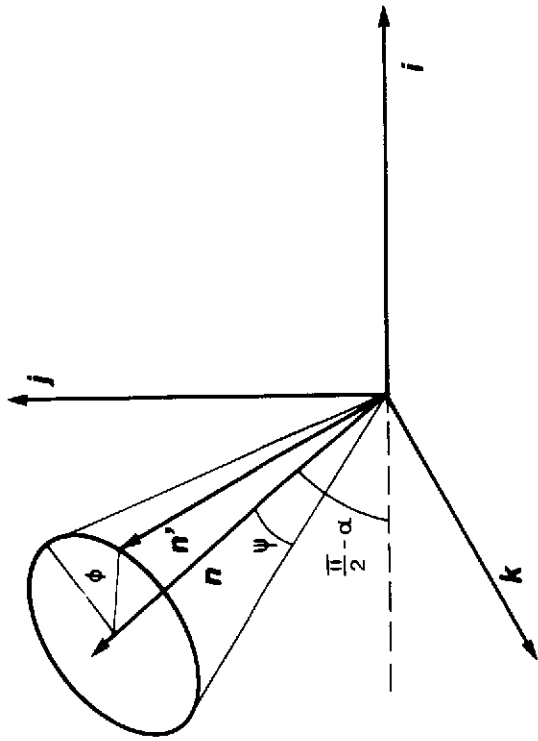


Fig. 2

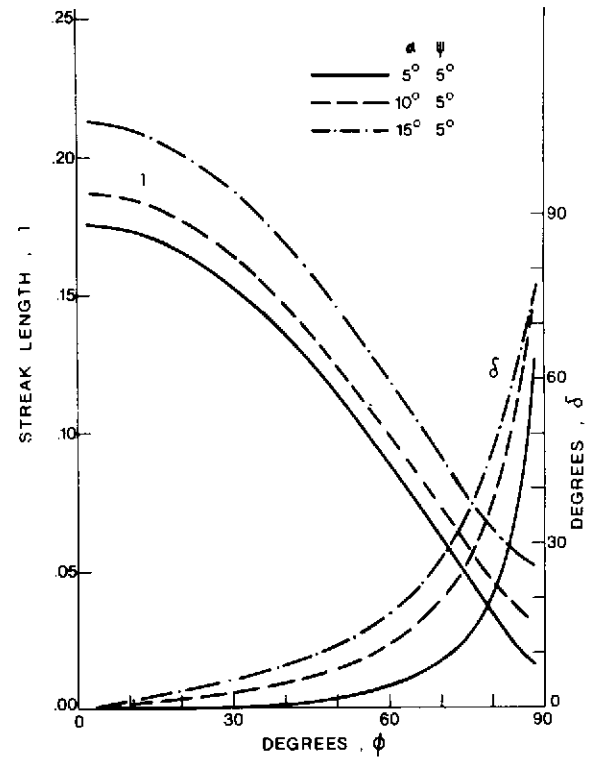


Fig. 3

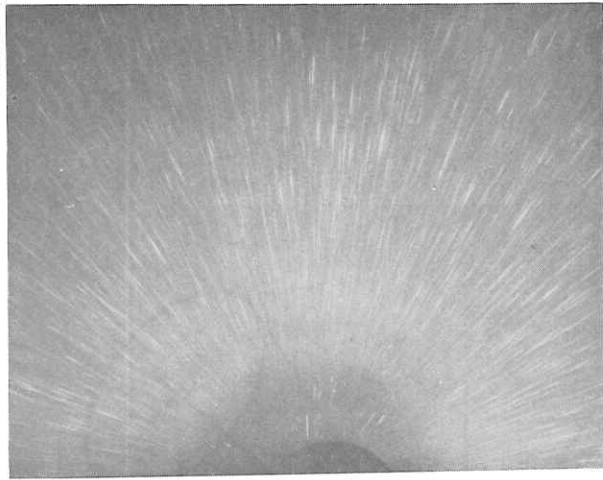


Fig. 4

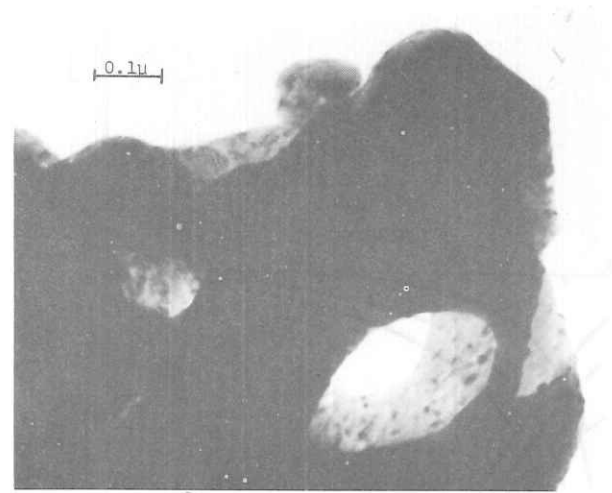


Fig. 6

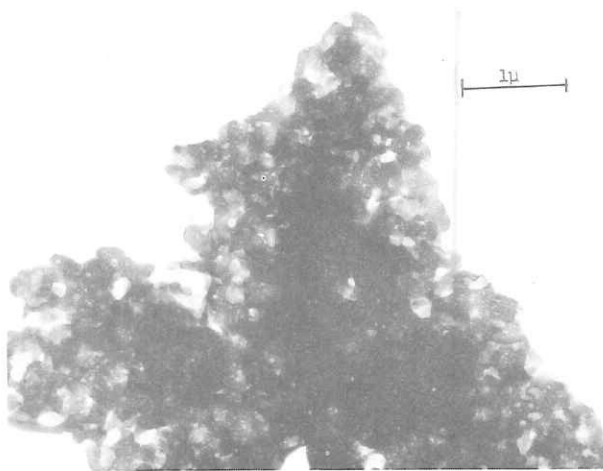


Fig 5

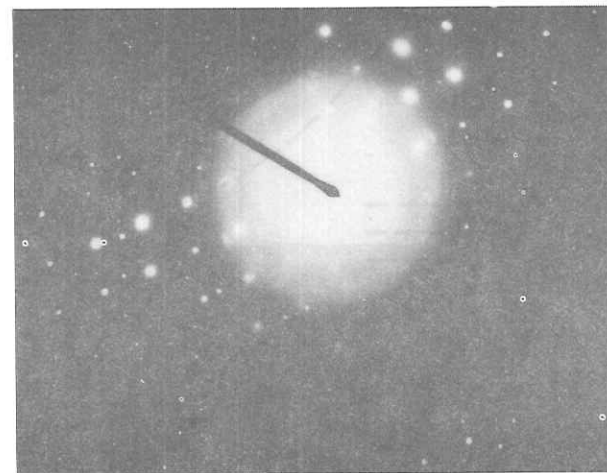


Fig. 7



Fig. 8

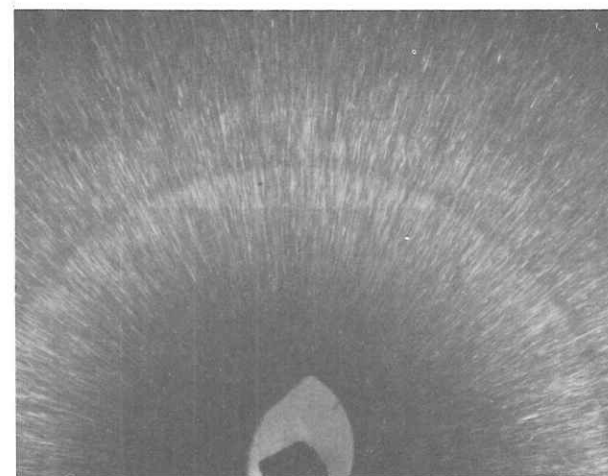


Fig. 10

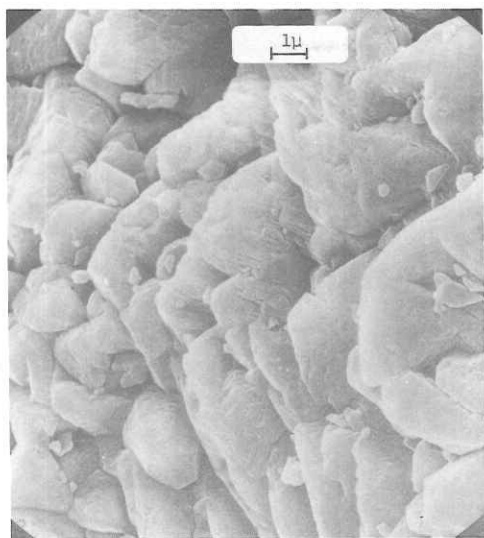


Fig. 9

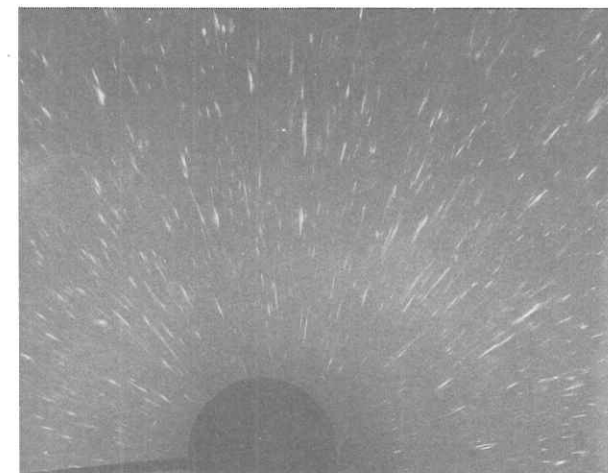


Fig. 11

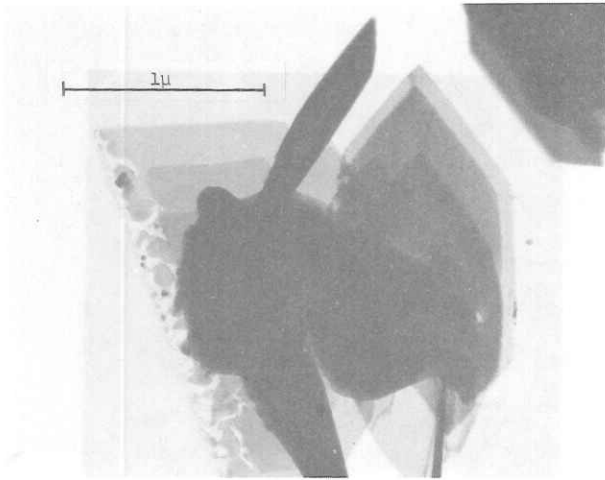


Fig. 12



Fig. 13

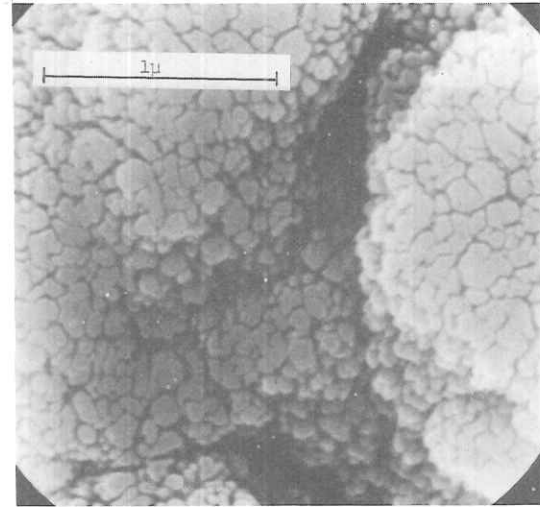


Fig. 14

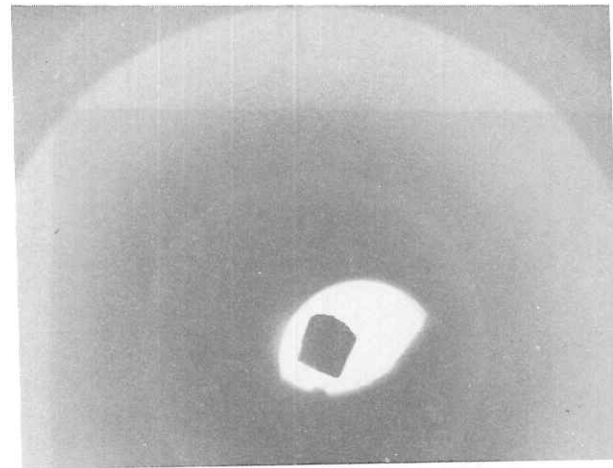


Fig. 15